RESEARCH ARTICLE SUMMARY

NEURODEVELOPMENT

Coordinated control of neuronal differentiation and wiring by sustained transcription factors

Mehmet Neset Özel*, Claudia Skok Gibbs, Isabel Holguera, Mennah Soliman, Richard Bonneau*, Claude Desplan*

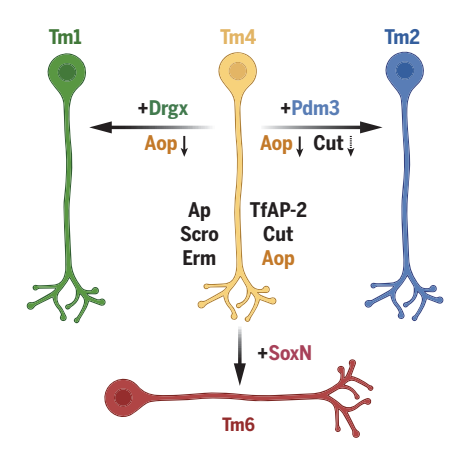
INTRODUCTION: Neurons are by far the most diverse of all cell types in animals, to the extent that "cell types" in mammalian brains are still mostly heterogeneous groups, and there is no consensus definition of the term. The *Drosophila* optic lobes, with approximately 200 well-defined cell types, provides a tractable system with which to address the genetic basis of neuronal type diversity. We previously characterized the distinct developmental gene expression program of each of these types using single-cell RNA sequencing (scRNA-seq), with one-to-one correspondence to the known morphological types.

RATIONALE: The identity of fly neurons is determined by temporal and spatial patterning mechanisms in stem cell progenitors, but it remained unclear how these cell fate decisions are implemented and maintained in postmitotic neurons. It was proposed in Caenorhabditis elegans that unique combinations of terminal selector transcription factors (TFs) that are continuously expressed in each neuron control nearly all of its type-specific gene expression. This model implies that it should be possible to engineer predictable and complete switches of identity between different neurons just by modifying these sustained TFs. We aimed to test this prediction in the Drosophila visual system.

RESULTS: Here, we used our developmental scRNA-seq atlases to identify the potential terminal selector genes in all optic lobe neurons. We found unique combinations of, on average, 10 differentially expressed and stably maintained (across all stages of development) TFs in each neuron. Through genetic gain- and loss-of-function experiments in postmitotic neurons, we showed that modifications of these selector codes are sufficient to induce predictable switches of identity between various cell types. Combinations of terminal selectors jointly control both developmental (e.g., morphology) and functional (e.g., neurotransmitters and their receptors) features of neurons.

The closely related Transmedullary 1 (Tm1), Tm2, Tm4, and Tm6 neurons (see the figure)

share a similar code of terminal selectors, but can be distinguished from each other by three TFs that are continuously and specifically expressed in one of these cell types: Drgx in Tm1, Pdm3 in Tm2, and SoxN in Tm6. We showed that the removal of each of these selectors in these cell types reprograms them to the default Tm4 fate. We validated these conversions using both morphological features and molecular markers. In addition, we performed scRNAseq to show that ectopic expression of pdm3 in Tm4 and Tm6 neurons converts them to neurons with transcriptomes that are nearly indistinguishable from that of wild-type Tm2 neurons. We also show that Drgx expression in Tm1 neurons is regulated by Klumpfuss, a TF expressed in stem cells that instructs this fate in progenitors, establishing a link between the regulatory programs that specify neuronal fates and those that implement them. We identified an intronic enhancer in the Drgx locus whose chromatin is specifically accessible in Tm1 neurons and in which Klu motifs are enriched. Genomic deletion



Terminal selectors enable predictive cell fate reprogramming. Tm1, Tm2, Tm4, and Tm6 neurons of the *Drosophila* visual system share a core set of TFs continuously expressed by each cell type (simplified). The default Tm4 fate is overridden by the expression of a single additional terminal selector to generate Tm1 (*Drgx*), Tm2 (*pdm3*), or Tm6 (*SoxN*) fates.

of this region knocked down Drgx expression specifically in Tm1 neurons, leaving it intact in the other cell types that normally express it. We further validated this concept by demonstrating that ectopic expression of Vsx (visual system homeobox) genes in Mil5 neurons not only converts them morphologically to Dm2 neurons, but also leads to the loss of their aminergic identity.

Our results suggest that selector combinations can be further sculpted by receptor tyrosine kinase signaling after neurogenesis, providing a potential mechanism for postmitotic plasticity of neuronal fates. Finally, we combined our transcriptomic datasets with previously generated chromatin accessibility datasets to understand the mechanisms that control brain wiring downstream of terminal selectors. We built predictive computational models of gene regulatory networks using the Inferelator framework. Experimental validations of these networks revealed how selectors interact with ecdysone-responsive TFs to activate a large and specific repertoire of cell surface proteins and other effectors in each neuron at the onset of synapse formation. We showed that these network models can be used to identify downstream effectors that mediate specific cellular decisions during circuit formation. For instance, reduced levels of cut expression in Tm2 neurons, because of its negative regulation by pdm3, controls the synaptic layer targeting of their axons. Knockdown of cut in Tm1 neurons is sufficient to redirect their axons to the Tm2 layer in the lobula neuropil without affecting other morphological features.

CONCLUSION: Our results support a model in which neuronal type identity is primarily determined by a relatively simple code of continuously expressed terminal selector TFs in each cell type throughout development. Our results provide a unified framework of how specific fates are initiated and maintained in postmitotic neurons and open new avenues to understanding synaptic specificity through gene regulatory networks. The conservation of this regulatory logic in both C. elegans and Drosophila makes it likely that the terminal selector concept will also be useful in understanding and manipulating the neuronal diversity of mammalian brains.

The list of author affiliations is available in the full article online. *Corresponding author. Email: no24@nyu.edu (M.N.Ö.); rb133@nyu.edu (R.B.); cd38@nyu.edu (C.D.) Cite this article as M. N. Özel et al., Science 378, eadd1884 (2022), DOI: 10.1126/science.add1884



READ THE FULL ARTICLE AT

https://doi.org/10.1126/science.add1884

RESEARCH ARTICLE

NEURODEVELOPMENT

Coordinated control of neuronal differentiation and wiring by sustained transcription factors

Mehmet Neset Özel¹*, Claudia Skok Gibbs^{2,3}, Isabel Holguera¹, Mennah Soliman¹, Richard Bonneau^{1,2,3}*, Claude Desplan^{1,4}*

The large diversity of cell types in nervous systems presents a challenge in identifying the genetic mechanisms that encode it. Here, we report that nearly 200 distinct neurons in the *Drosophila* visual system can each be defined by unique combinations of on average 10 continuously expressed transcription factors. We show that targeted modifications of this terminal selector code induce predictable conversions of neuronal fates that appear morphologically and transcriptionally complete. Cis-regulatory analysis of open chromatin links one of these genes to an upstream patterning factor that specifies neuronal fates in stem cells. Experimentally validated network models describe the synergistic regulation of downstream effectors by terminal selectors and ecdysone signaling during brain wiring. Our results provide a generalizable framework of how specific fates are implemented in postmitotic neurons.

eurons are by far the most diverse of all cell types in animals. Understanding the molecular mechanisms that produce this diversity is a central goal of neurobiology. The *Drosophila* brain provides a tractable system to approach this challenge because of its manageable size and genetically hardwired development. The optic lobes constitute two-thirds of the fly brain, and each of their neuropils—the lamina, medulla, lobula, and lobula plate (Fig. 1A)-is divided into ~800 columns, corresponding to the same number of ommatidia (unit eves) in the retina. Because of this retinotopic organization with multiple repeats of the same circuits, most neuronal types are present in high numbers of cells per brain. We previously completed a large single-cell RNA sequencing (scRNA-seq) atlas of the optic lobes, resolving ~200 cell types that we consistently tracked across six time points from the early pupal stages to adult (1). Almost all annotated clusters in this atlas corresponded to a distinct neuronal type with unique morphology (2). This strongly suggests that most of our clusters represent biologically homogeneous groups, giving us access to the cell-type-specific transcriptome of every neuron throughout its development.

The identity of optic lobe neurons is specified deterministically by their progenitors during neurogenesis, which occurs from late larval stages (L3) until ~20% of pupal development (P20) (3). Neurons from the medulla

neuropil are produced from a neuroepithelium called the outer proliferation center, which is progressively converted into neuroblasts that asymmetrically divide multiple times, each time self-renewing and producing an intermediate progenitor that divides once to generate two different neurons (4). Neurons are diversified by the intersection of three patterning mechanisms: (i) compartmentalization of the neuroepithelium into at least eight spatial regions by transcription factors (TFs) and signaling molecules (5), (ii) sequential expression of at least 11 temporal TFs (tTFs) in neuroblasts (6), and (iii) Notch signaling between sister neurons (7). Similar patterning mechanisms are also used in other parts of the fly brain, as well as mammalian neural stem cells to generate diversity [reviewed in (8)]. However, most spatial and tTFs are not maintained in neurons (6), so it is not clear how these cell fate decisions are implemented and maintained in postmitotic neurons.

Much of our knowledge about neuronal identity control originates from Caenorhabditis elegans. The terminal selector hypothesis (9) posits that type-specific gene expression in neurons is controlled by combinations of TFs that are continuously maintained in each neuron throughout its life. Terminal selectors control both developmental features such as synaptic connectivity (10) and functional features such as neurotransmitter identity (11), but they are largely not required for pan-neuronal gene expression programs (12). This model also implies that individual selectors do not specialize in distinct phenotypic features of a neuron. Although a few TFs that could function as terminal selectors have been identified in mammalian neurons (13-15), it remains unclear how generally applicable this regulatory logic is beyond the relatively simple nervous system of worms. Moreover, the ultimate test of this model, i.e., the predictive and complete transformation of one neuronal type into another through targeted modification of its selector code, has been difficult to assess, even in *C. elegans* (16).

Results

Terminal selectors of optic lobe neurons

To determine whether a sustained code of TFs maintains the identity of each neuron throughout development, we sought to identify the combinations of candidate terminal selectors expressed in each of the 174 neuronal clusters in our scRNA-seq atlas (1). We determined the sets of TFs continuously expressed in each cluster throughout all six stages of development (P15 to adult), excluding those expressed in all clusters (pan-neuronal or ubiquitous genes; see the materials and methods). We found, on average, unique combinations of 10 such genes per cluster, representing 95 TFs in total (fig. S1A and table S1); 72 of these TFs were expressed in fewer than 25 clusters (fig. S1B). Homeobox genes were enriched in this list (fig. S1C), but unlike in the C. elegans nervous system (17), they were not sufficient to uniquely define every neuron. Furthermore, whereas the selectors could delineate developmentally related lineages, e.g., from lamina or the inner proliferation center (fig. S2A), homeobox genes alone could not (fig. S2B).

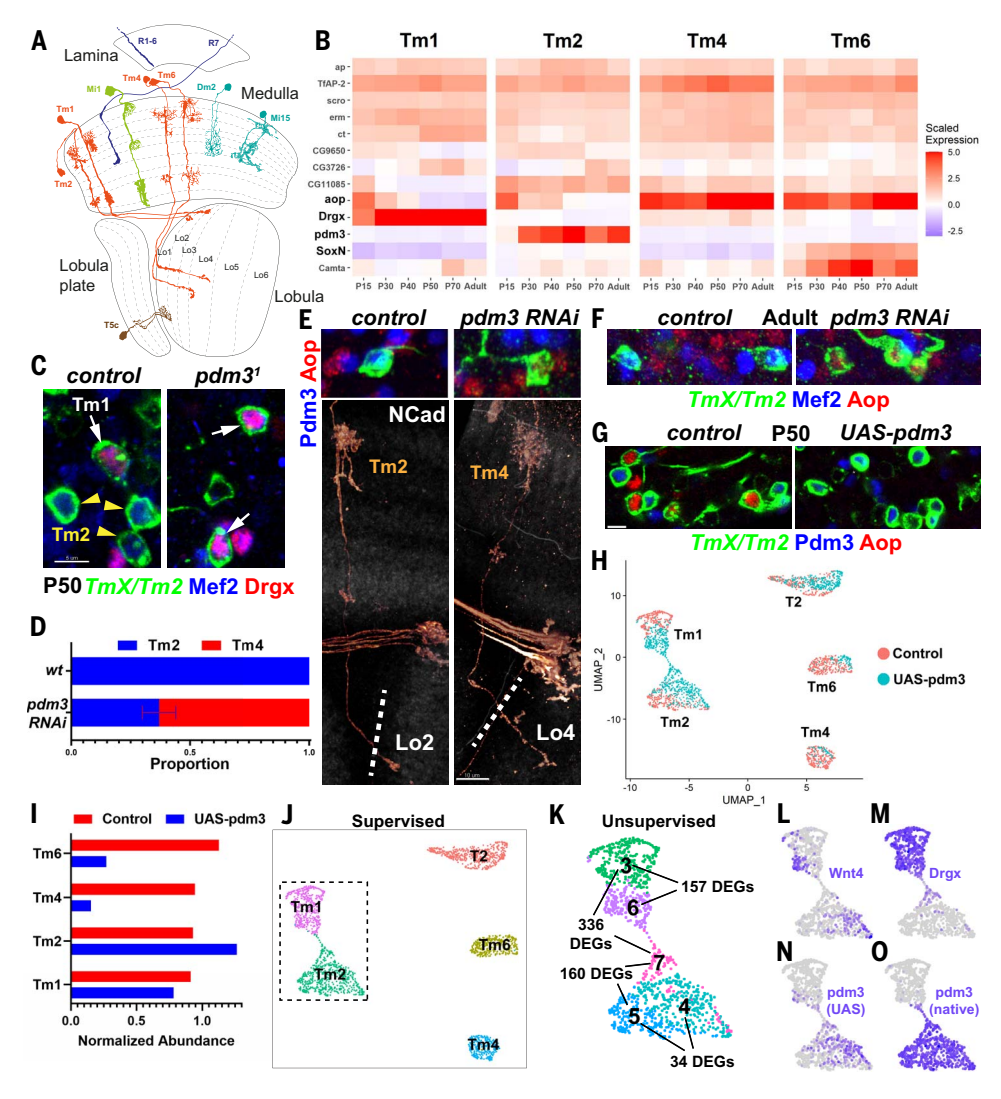
The terminal selector hypothesis predicts that if continuously maintained TFs are primarily responsible for cell-type-specific neuronal differentiation, then it should be possible to engineer complete switches of identity between different neurons by modifying these TFs alone. All genes that were previously reported to interfere with neuronal type identity in the optic lobe, including bsh, hth, drifter (vvl), Lim1, erm, SoxN, and Sox102F (18-22), were indeed candidate selectors for the respective neurons (fig. S1A). However, these studies generally reported disruptions rather than switches of morphological identity; for example, loss of hth/bsh in Mi1 results in an incomplete conversion to "Tm1-like" neurons (19), likely because Tm1 differs from Mi1 by the expression of the additional selectors Drgx and TfAP-2. It remains challenging to simultaneously perturb more than one or two genes at once using classical genetic methods. To provide definitive evidence for the sufficiency of terminal selectors in determining neuronal type identity, we looked for groups of closely related neurons with selector codes that differed only by one or two genes, in which complete conversions from one cell type to another may be feasible.

Transmedullary (Tm) neurons 1, 2, and 4 and an unidentified cluster (#62) have nearly indistinguishable transcriptomes shortly after their terminal division at P15 (1), suggesting a

¹Department of Biology, New York University, New York, NY 10003, USA. ²Flatiron Institute, Center for Computational Biology, Simons Foundation, New York, NY 10010, USA. ³Center for Data Science, New York University, New York, NY 10003, USA. ⁴New York University Abu Dhabi, Saadiyat Island, Abu Dhabi, United Arab Emirates.

^{*}Corresponding author. Email: no24@nyu.edu (M.N.Ö.); rb133@nyu.edu (R.B.); cd38@nyu.edu (C.D.)

Fig. 1. Pdm3 instructs complete switches of **neuronal fates.** (A) D. melanogaster optic lobe in cross section, with drawings of select cell types. Image was adapted in part from (2). (B) Developmental (scaled) expression patterns (1) of all genes that are candidate selectors in any of the displayed cell types. (C) FRT40A and pdm3¹ MARCM clones labeled with TmX/Tm2-Gal4 and CD4-tdGFP in P50 brains (maximum projection), with anti-Mef2 shown in blue and anti-Drgx in red. n = 8 control and n = 4 mutant brains. (**D** to F) TmX/Tm2-Gal4 driving pdm3 RNAi and CD4-tdGFP (flip-out). (D) Quantification of (E) and (F). n = 54/6 control and n = 96/8 RNAi neurons/brains, P < 0.0001. Error bar indicates SEM. (E) Three-dimensional (3D) reconstructions of GFP (bottom) or maximum projections (top) for the same representative adult neurons in each condition, with anti-NCad shown in white, anti-Pdm3 in blue, and anti-Aop in red. The dashed lines indicate the border of the lobula neuropil based on NCad staining. (F) Same as (E), top, but with anti-Mef2 instead of Pdm3. (G) TmX/Tm2-Gal4 driving UAS-pdm3 and CD4-tdGFP (flip-out). Maximum projections of somas in P50 medulla cortex, with anti-Pdm3 shown in blue and anti-Aop shown in red. n = 129 control and n = 118 pdm3 neurons. Scale bars: (C) and (E), top. (F), and (G), 5 um: (E), bottom, 10 μm. (H to O) scRNA-seq of FACSed neurons [same experiment as in (G)]. UMAP visualizations were calculated using top six principal components (PCs). Cells are colored according to library (condition) of origin (H), supervised classifications (J). unsupervised clustering [(K) inset only, see also fig. S4A], and the log-normalized



expression of indicated genes [(L) to (0)]. (I) Numbers of Tm neurons in each library divided by the numbers of T2 neurons.

very close developmental relationship. We annotated cluster 62 as being composed of Tm6 neurons on the basis of its expression of the unique combination of aop, SoxN, and Wnt10 (fig. S3, A to C). Although these Tms share similar overall morphology, adult neurons are readily distinguishable from one another by their distinct dendritic shapes, as well as the different target layers of their axons in the lobula (Fig. 1A). Analysis of candidate selector expression in these clusters across development (Fig. 1B) revealed that the four neurons indeed share a similar code: ap, TfAP-2, scro, erm, and ct are continuously expressed in all four clusters. CG9650, CG3726, CG11085, and aop could also be found in all four Tm neurons at some point during development, although they were only transiently expressed in some of them. Camta is expressed at much higher levels in Tm6 but is also detected in the others. Among these four neurons, Drgx is specific to Tm1, pdm3 to Tm2, and SoxN to Tm6, whereas there are no candidate selectors exclusive to Tm4. Therefore, these TFs that are each continuously and specifically expressed in one of these types are strong candidates to differentially specify their fates.

Pdm3 instructs transcriptionally complete neuronal fate conversions

Because *pdm3* is the only TF that continuously distinguishes Tm2 from Tm4 (Fig. 1B), the terminal selector code predicts that its loss should reprogram Tm2 neurons to Tm4 fate. *R71F05-Gal4* is expressed in all four Tm neurons (1, 2, 4, and 6) until P50; however, it is only maintained in Tm2 in adults (fig. S3D, *TmX/Tm2-Gal4*). Using this driver, we generated MARCM (23) clones of a *pdm3*-null allele (24). No mutant Tm neurons were recovered in adult brains, suggesting that Tm2 were not specified properly (fig. S3E). *Mef*2 is an effector (downstream) TF that is normally expressed specifically in both

Tm1 and Tm2 after P40 (Fig. 1C and fig. S7J). At P50, we observed that the only remaining Mef2⁺ Tm neurons in *pdm3*¹ clones were Tm1 that expressed Drgx (Fig. 1C), indicating that Tm2 were either lost or converted to another fate. Unlike the mutant, upon RNA interference (RNAi) knockdown of pdm3 using TmX/Tm2-Gal4, 65% of Tm2s that retained the expression of the driver in adult brains were converted to neurons with Tm4 morphology, as characterized by wider dendritic arbors that were symmetrical around the main fiber of the neuron and axons targeting the deeper lobula layer 4 (Fig. 1, D and E; compare with Fig. 1A). It is likely that the knockdown retains low levels of Pdm3 in Tm2 that are sufficient to maintain expression of TmX/Tm2-Gal4 but are insufficient for instructing the Tm2 fate. These Tm4-looking neurons did not express Mef2 and instead expressed the putative Tm4 selector Aop (Fig. 1, E and F).

We then investigated whether ectopic expression of pdm3 in Tm4 and Tm6 could be sufficient to convert them to Tm2 fate. We used TmX/Tm2-Gal4 to express UAS-pdm3. short (25) and found that >90% of Aop+ neurons (Tm4 and Tm6) were eliminated at P50 (Fig. 1G), suggesting that they had been lost or converted. To address the completeness of these conversions at P50, when the neurons have not fully acquired their adult morphology but display the greatest transcriptomic diversity (1), we analyzed their gene expression with scRNA-seq. Because the driver weakly labels several other cell types (fig. S4A and see the materials and methods), we only retained the cells classified as Tm1, Tm2, Tm4, or Tm6 by a neural network trained on our reference atlas (1), in addition to those classified as T2 that are also strongly labeled by TmX/Tm2-Gal4 (Fig. 1, H and J). T2 neurons, like Tm2, natively express pdm3, and thus they should not be affected by this perturbation and serve as an internal control. We observed a depletion of Tm4 and Tm6 in the UAS-pdm3 library compared with control and an increase in the number of Tm2s (Fig. 1I), indicating that ectopic pdm3 converts Tm4 and Tm6 to Tm2. We noted that the increased number of Tm2s upon pdm3 overexpression was not sufficient to fully account for the lost Tm4s and Tm6s. Some optic lobe neurons are known to be generated in excess, followed by widespread apoptosis in the first half of pupal development (26). Staining against cleaved Dcp-1, an activated caspase that marks dying cells (27), indeed showed a significantly increased rate of apoptosis in brains overexpressing pdm3 at P25 (fig. S4, B and C), whereas no Tm2 somas (GFP⁺Pdm3⁺) were stained with Dcp-1 in the control brains. Together, these results suggest that when excess Tm2s are produced through conversions from Tm4 and Tm6, this is compensated for by increased cell death. This mechanism potentially helps to ensure that only one Tm neuron of each type is present per column in wild-type brains.

To distinguish the wild-type Tm2 neurons from those converted from another cell type, we performed unsupervised clustering on the dataset. This revealed heterogeneous populations among the cells classified as Tm1 and Tm2 (fig. S4D and Fig. 1K). Tm2 subclusters 4 and 5 were extremely similar, with only 34 significant differentially expressed genes (DEGs). Most of these differences were consistent with markers of the control Tm4 and Tm6 clusters (fig. S4E), including the strongest one, Wnt4, which was found in cluster 4 (Fig. 1L). We recently showed that Wnt4 is expressed in ventral Tm4 and Tm6, but not in Tm2 (1), suggesting that cells in cluster 4 were converted neurons that had retained these markers from their initial specification as Tm4 or Tm6. Nevertheless, these differences between the converted and "original" Tm2s were minimal compared with the >700 DEGs observed between wild-type Tm2 and Tm4 at this stage (Table S2). We therefore conclude that conversion from Tm4 or Tm6 fate to Tm2 fate induced by ectopic *pdm3* appears complete.

The third subgroup of the cells classified as Tm2, cluster 7, consisted entirely of cells from the UAS-pdm3 library and expressed the Tm1 selector Drgx (Fig. 1M), suggesting that they were originally Tm1s converted to a Tm2-like state. These were still significantly different from cluster 5 (wild-type Tm2), with 160 DEGs (Fig. 1K). The cells classified as Tm1 were clustered into two groups: cluster 6, which was made entirely of cells from the UAS-pdm3 library and was significantly different from the second group, cluster 3, which consisted essentially of wild-type Tm1s (Fig. 1, H and K). Thus, both clusters 6 and 7 contained Tm1s with ectopic pdm3. Uniform manifold approximation and projection (UMAP) visualization showed a thin stripe of cells bridging the Tm1-like (cluster 6) and Tm2-like (cluster 7) states. We observed that although both clusters 6 and 7 displayed reads coming from the UAS-pdm3 construct, as expected (Fig. 1N), cluster 7 also expressed pdm3 from the native locus (Fig. 10). We thereby conclude that the amount of protein produced from the UAS construct is insufficient for conversion into Tm2, and instead Pdm3 must autoactivate above a certain threshold. Once this threshold is reached, Pdm3 quickly drives Tm1, Tm4, and Tm6 to a Tm2-like state; however, this conversion is incomplete in Tm1 (cluster 7) because Drgx remains expressed. Morphologically, Tm1s overexpressing pdm3 appeared normal in adults (fig. S3F), suggesting that the 157 DEGs between clusters 3 and 6 are not important for morphology.

In summary, *pdm3* is necessary and sufficient to instruct the fate choice between Tm2 and Tm4 neurons, as predicted by the terminal selector code. Its loss results in morphological conversion of Tm2 into Tm4, and its ectopic expression can induce essentially complete transcriptomic conversions of Tm4 and Tm6 to Tm2 fate. It is also an upstream repressor of the Tm4 and Tm6 selector *aop* (Fig. 1, E and G).

The Tm1 selector Drgx is regulated by Klumpfuss

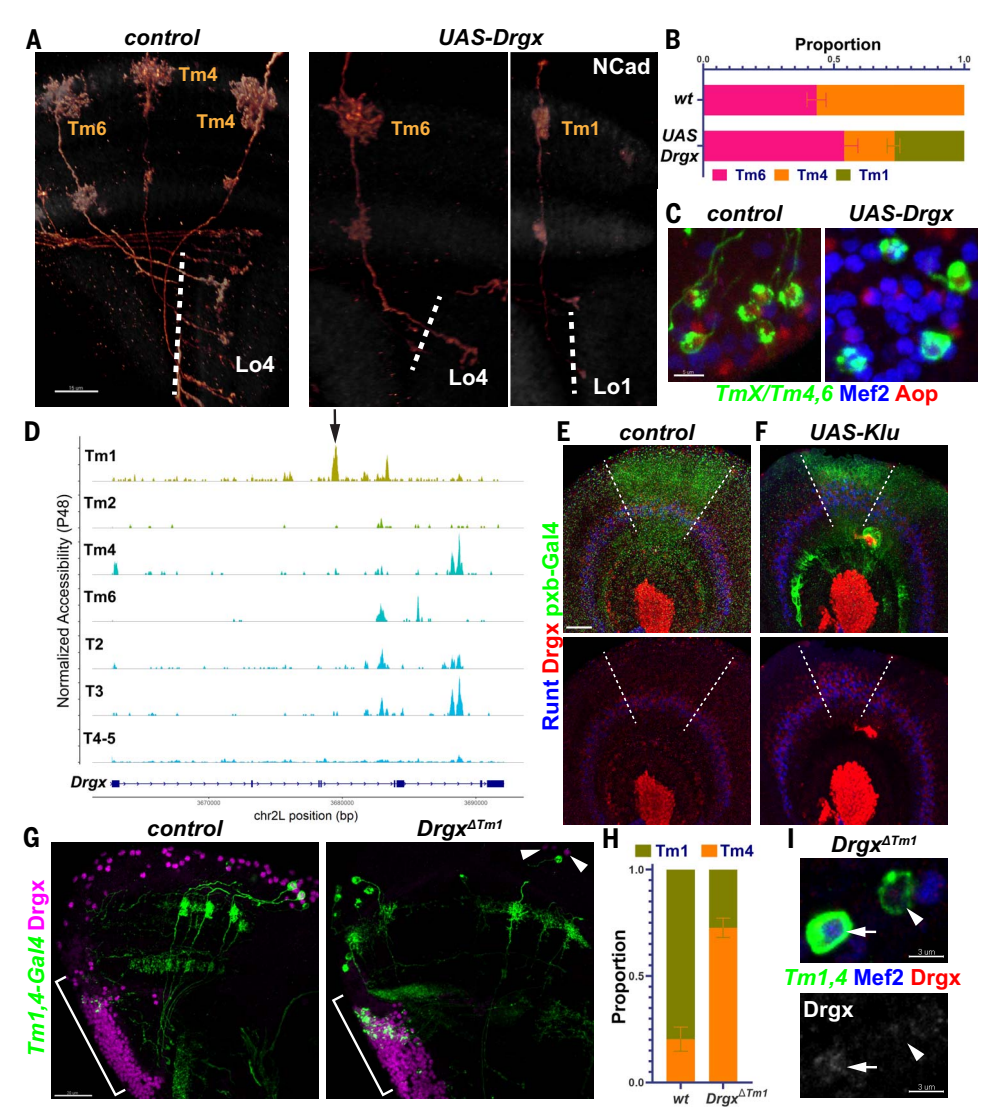
Similar to *pdm3* in Tm2, Drgx is the only TF that continuously distinguishes Tm1 from Tm4 (Fig. 1B). We ectopically expressed *Drgx* using *R35H01-Gal4*, which is expressed in all four Tm neurons until P50 but is only maintained in Tm4 and Tm6 in adults (fig. S5, A and B, *TmX/Tm4,6-Gal4*). In these adult brains, the proportion of Tm6 remained unchanged, but most Tm4s were converted into Tm1s, characterized by much narrower dendritic ar-

bors and axons terminating in the first layer of the lobula (Fig. 2, A and B, and see Fig. 1A). The converted neurons also lost Aop expression and instead expressed Mef2 (a Tm1 and Tm2 marker) (Fig. 2C). Some of the converted neurons displayed morphological features atypical of Tm1, such as targeting to the Lo2 layer instead of Lo1 (fig. S5C). We suspect that this partial expressivity is caused by low Gal4 expression from TmX/Tm4,6-Gal4. Moreover, the fact that this driver is expressed at even weaker levels in Tm6 compared with Tm4 (fig. S5B) might explain our failure to affect Tm6 fate. Loss of Drgx (described below) resulted in conversion of Tm1s into Tm4s (Fig. 2, G and H). Thus, *Drgx* specifies the Tm1 fate: It can repress aop and mediate the conversion of Tm4 into Tm1, as predicted by the selector code.

Neither *Drgx* nor *pdm3* is expressed in the progenitors (neuroblasts) of Tm neurons (6), implying that their postmitotic expression in specific neurons is instructed by tTFs in the neuroblasts. To investigate how this is controlled, we used a single-nucleus assay for transposase-accessible chromatin sequencing (snATAC-seq) dataset of the developing *Drosophila* brain (28). We identified the cells belonging to optic lobe neurons at adult, P48, and P24 stages, and then reclustered and annotated them using our scRNA-seq atlas (1) as a reference (fig. S6, A to D, and materials and methods). We found a putative enhancer in the fourth intron of Drgx that was specifically accessible in Tm1 throughout development (fig. S6E) but was not accessible in the other Tm neurons or in T2, T3, T4, or T5 neurons, which also express Drgx (Fig. 2D). We found that the only enriched binding motifs for any of the TFs expressed in the optic lobe (E-value < 100; see the materials and methods) within this 700 base-pair region belonged to the tTF Klumpfuss (Klu). Klu is expressed at higher levels in neuroblasts during early temporal windows, when Tm1s are generated, and its overexpression in neuroblasts can expand Runt⁺ neurons (29) that are likely born in the same temporal window as Tm1 (Fig. 2E) (6). Thus, Klu might also regulate Drgx expression. Indeed, Klu overexpression using pxb-Gal4, which is expressed in the central region of the neuroepithelium (Fig. 2, E and F, dashed lines), resulted in the expansion of Drgx⁺ neurons (i.e., Tm1) in this region, similar to Runt (Fig. 2F). We therefore conclude that Klu expression in neuroblasts helps to specify Tm1 from an early temporal window by activating the selector Drgx in their neuronal progeny.

Next, we investigated whether Drgx expression is regulated by this enhancer element by engineering a CRISPR deletion ($Drgx^{\Lambda Tm1}$; see the materials and methods), which should function as a conditional mutant specifically

Fig. 2. The Tm1 selector Drgx is regulated by Klumpfuss. (A to C) TmX/Tm4,6-Gal4 driving UAS-Drgx and CD4-tdGFP (flip-out). (A) 3D reconstructions of GFP for representative adult neurons, with anti-NCad shown in white. Dashed lines mark the border of lobula neuropil. (B) Quantification of (A). n = 92/4 control and n = 45/6 Drgx neurons/brain, P = 0.0003. (C) Same as (A) but with maximum projections of somas. anti-Mef2 is shown in blue and anti-Aop is shown in red. (D) Aggregated accessibility tracks of Drgx locus from the normalized snATAC-seg data at P48 (28). Arrow indicates the Tm1-specific enhancer deleted in (G) to (I). (E and F) pxb-Gal4 driving CD8-GFP and UAS-Klu [(F), n = 5 brains] in L3 optic lobes, with anti-Runt shown in blue and anti-Drgx shown in red. Dashed lines mark the borders of driver expression. (G to I) Tm1,4-Gal4 driving CD4-tdGFP (flip-out) in heterozygous (control) or homozygous Drgx^{∆Tm1} mutants. (G) Maximum projections of adult optic lobes. Anti-Drgx is shown in magenta. Brackets mark the location of the lobula plate cortex (T2 to T5 neurons). Arrowheads indicate glia (see also fig. S5E) that maintain Drgx expression in the mutants. (H) Quantification of (G) (see also fig. S5D). Tm1 were normally observed more frequently than Tm4 because the driver expression is much lower in Tm4. n = 57/6 control and $n = 181/10 \ Drgx^{\Delta Tm1}$ neurons/brains. P < 0.0001. (I) Same as (G), but with somas. Anti-Mef2 is shown in blue and anti-Drgx is shown in red, or only anti-Drgx in grayscale (bottom). The arrow indicates a Tm1 nucleus, and the arrowhead indicates a Tm4 nucleus. Scale bars: (A), (E), and (F). 15 um; (C). 5 um; (G). 20 um; and (I). 3 um. Error bars indicate SEM.



in Tm1. 27b-Gal4 (30) is expressed in Tm1 and much more weakly in Tm4 (fig. S5D, Tm1,4-*Gal4*) throughout development. In $Drgx^{\Delta Tm1}$ mutant adults, Drgx expression in the medulla cortex (where all Tm somas are located) was almost completely lost (Fig. 2G), but it was still normally present in Repo⁺ perineurial glia (fig. S5E) at the surface of the brain (Fig. 2G, arrowheads) and in T neurons originating from the lobula plate (Fig. 2G, brackets). The observed ratio of Tm1 to Tm4 labeled by Tm1,4-Gal4 decreased significantly in the mutant brains (Fig. 2H). This was not caused by the death of Tm1s because we could observe no apoptotic Tm1s at P25 in either condition (fig. S5, F and G), suggesting instead that most Tm1s were converted to Tm4s. Furthermore, 69% of the few remaining Tm1s displayed abnormal morphological features such as disrupted dendritic arbors and/or axons reaching to deeper layers in the lobula (fig. S5D). Close examination of somas revealed that these neurons that maintained

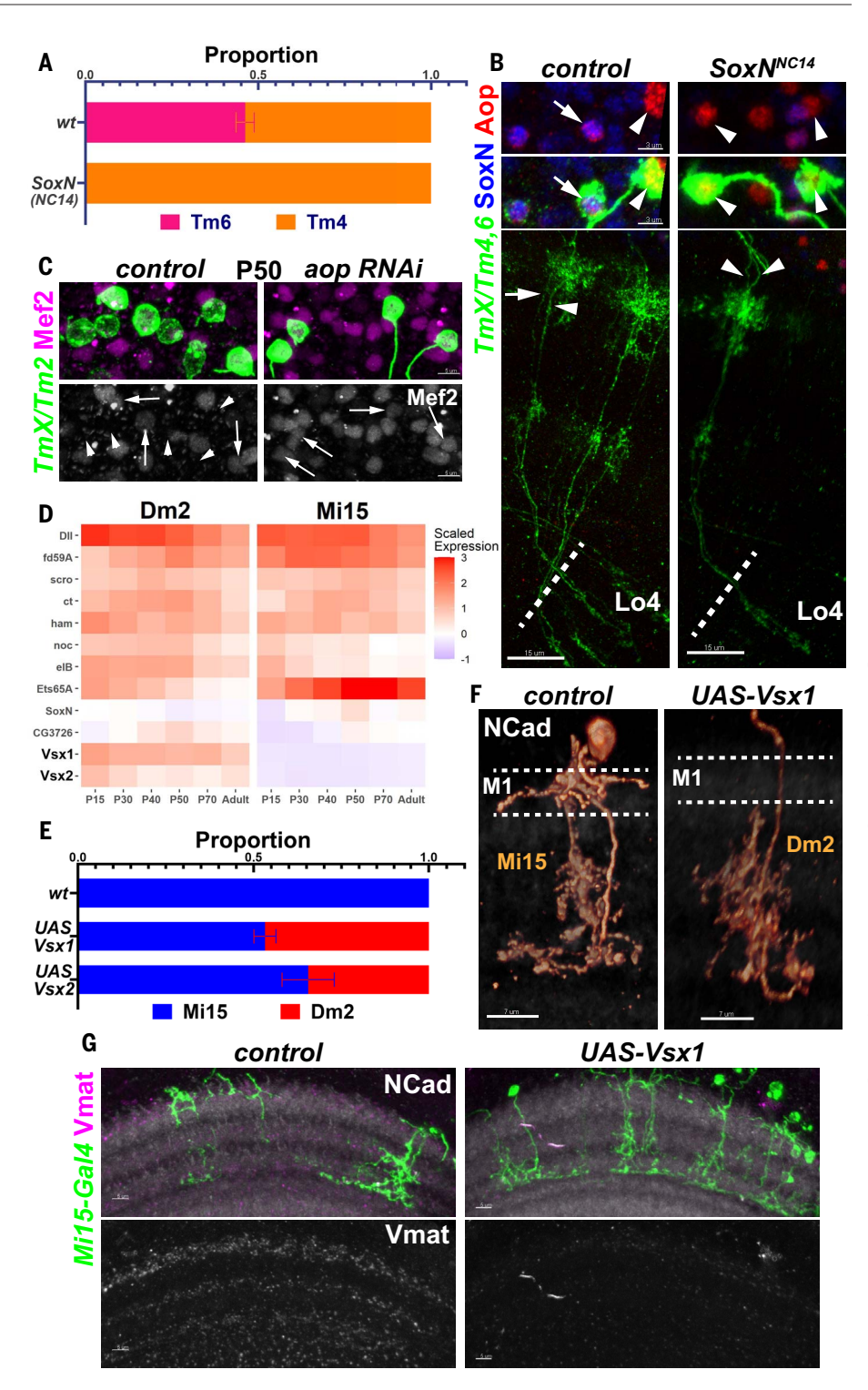
Mef2 (a Tm1 and Tm2 marker) still expressed Drgx at very low levels (Fig. 2I, arrow). In addition, Drgx expression was normal in $Drgx^{ATm1}$ mutants at the L3 stage (fig. S5H). These results suggest that there are other, partially redundant enhancers regulating Drgx that control its initial activation in newborn neurons, whereas the robust maintenance of expression in Tm1 requires this specific enhancer. Even though it is not maintained later, Klu could be priming this enhancer in newborn Tm1s to ensure the sustained expression of Drgx.

Selectors jointly control developmental and functional features

Similar to *Drgx* in Tm1 and *pdm3* in Tm2, *SoxN* is the sole candidate selector distinguishing Tm6 from Tm4 (Fig. 1B). In control MARCM clones marked with *TmX/Tm4,6-Gal4*, we observed roughly equal numbers of adult Tm4 and Tm6. By contrast, only Tm4s could be observed in the *SoxN*-null mutant (*31*) clones (Fig. 3A). All four Tm neurons are

unicolumnar neurons produced by all neuroblasts; therefore, a given column should contain one Tm4 and one Tm6 generated from the same neuroblast (5). We consistently observed Tm4 and Tm6 neurites occupying the same column in sparse control MARCM neuroblast clones (Fig. 3B). However, these clones consisted of two Tm4s in SoxN mutants (Fig. 3B), indicating that the loss of SoxN converted Tm6 to Tm4 rather than eliminating them. However, columns with these pairs were rare, suggesting that the extra Tm4s often undergo apoptosis, as shown above for Tm2. Overexpressing SoxN using TmX/Tm4,6-Gal4 did not convert Tm4s to Tm6 fate (fig. S7A). This is again likely caused by the weak Gal4 driver, because the amount of SoxN protein detected in these Tm4 nuclei was an order of magnitude lower than in wild-type Tm6 nuclei (fig. S7A, insets). Thus, we could engineer predictable switches of type identity between all four Tm neurons guided solely by a code of sustained transcription factors.

Fig. 3. Selectors jointly control developmental and functional features. (A and B) FRT40A and SoxN^{NC14} MARCM clones labeled with TmX/ Tm4,6-Gal4 and CD4-tdGFP in adult brains. (A) Quantification of (B) based on Aop-only (Tm4) and Aop+SoxN (Tm6) neurons. n = 225/9 control and $n = 258/10 \text{ SoxN}^{\text{NC14}}$ neurons/brains, P < 0.0001. No neurons with Tm6 morphology were observed in the mutant clones. (B) Maximum projections, with anti-SoxN shown in blue and anti-Aop shown in red, displaying the neurites (bottom) and the somas (top) of the same two neurons. Arrows indicate Tm6. and arrowheads indicate Tm4. (C) TmX/Tm2-Gal4 driving aop RNAi (n = 6 brains) and CD4-tdGFP (flip-out). Maximum projections of somas at P50 with anti-Mef2 (top: magenta, bottom: white). Arrows indicate GFP+Mef2+ Tm neurons, and arrowheads indicate GFP+Mef2- Tm neurons (**D**) Developmental (scaled) expression patterns (1) of all genes that are candidate selectors in either of the displayed cell types. (E) Quantification of (F) and fig. S7D. Cells labeled by Mi15(R76F01)-Gal4 were identified on the basis of their morphology in each condition. n = 104/11 wild-type, n = 108/11UAS-Vsx1, and n = 24/4 UAS-Vsx2 neurons/brains, P < 0.0001 for change in Dm2 proportions in both conditions. Error bars indicate SEM. (F and G) Mi15-Gal4 driving UAS-Vsx1 and CD4-tdGFP (flip-out). (F) 3D reconstructions of GFP for representative adult neurons in each condition (see also Fig. 1A), with anti-NCad shown in white. Dashed lines mark the M1 layer where Mi15 arborizes but Dm2 does not. Also note that Mi15 has two descending branches, whereas Dm2 has one. (G) Maximum projections of adult optic lobes, with anti-NCad shown in white and anti-Vmat shown in magenta (top) and white (bottom). n = 4 control brains and n = 7 UAS-Vsx1 brains. Scale bars: (B), 15 μ m; (C) and (G), 5 μ m; (F), 7 μ m.



Combined, our results suggest that Tm4 is the default fate among these Tm neurons, which is overridden by Drgx in Tm1, by pdm3 in Tm2, and by SoxN in Tm6. aop is expressed in both Tm4 and Tm6, but it is repressed by Drgx in Tm1 and by pdm3 in Tm2. To address whether Aop also functions as a selector, we generated aop-null MARCM clones (32) and also performed RNAi knockdown using TmX/

Tm4,6-Gal4; in both cases, the driver was turned off (fig. S7, B and C). When we instead used TmX/Tm2-Gal4 to express aop RNAi, we observed that all Tm neurons at P50 (when this driver normally labels all four Tms) expressed the Tm1 and Tm2 marker Mef2 (Fig. 3C), indicating that aop is necessary for Tm4 and Tm6 identity. However, we could not determine the exact fate of these neurons,

i.e., whether they were eliminated or transformed to Tm1 or Tm2 fate, because both were labeled by the driver.

To further validate the terminal selector concept for functional features of neurons, we sought other neuronal types with selector codes that differ only by a few genes, and that also use different neurotransmitters. Dm2 and Mi15 are both cholinergic, but Mi15 are also the

only aminergic neurons in the optic lobe (33), expressing the vesicular monoamine transporter (Vmat). Both of these neurons express the candidate selectors Dll, fd59A, scro, ct, ham, noc, eIB, and Ets65A, but Vsx1 and Vsx2 are specific to Dm2 and are the only TFs that continuously distinguish the two cell types (Fig. 3D). Ectopic expression of either Vsx1 or Vsx2 using an Mi15-specific (early) driver was sufficient to convert them to Dm2 morphology (Fig. 3, E and F; fig. S7D; and see Fig. 1A). Vsx1 and Vsx2 could function redundantly because of their sequence similarity or they could crossactivate each other's expression. However, we did not observe Vsx2 protein in Mi15s ectopically expressing Vsx1 (fig. S7E), suggesting redundancy.

Next, we evaluated these conversions for more terminal features that are likely to be important for neurotransmission. We observed a drastic reduction in Vmat protein levels in the medulla upon Vsx1 overexpression in Mi15 (Fig. 3G). In addition, we investigated four neurotransmitter or modulator receptor genes that are differentially expressed between Mi15 and Dm2 clusters: 5-HT7, OctβIR, Or63a, and Dh44-R1 (fig. S7I). Using in situ hybridization, we observed that Mi15s overexpressing Vsx1 down-regulated Or63a and Dh44-R1 and they up-regulated 5-HT7 and $Oct\beta IR$ (fig. S7. F to H), as expected. These results show that Vsx genes function as terminal selectors in Dm2, controlling both morphological and functional features.

RTK signaling stabilizes the Tm selector network

Even though the mRNA of the Tm4/6-specific selector aop could be found in all four Tm neurons up to P40 (fig. S7J), Aop protein was no longer localized to Tm1 nuclei already by P25 (fig. S5F). This could be explained by a well-known posttranslational regulatory mechanism: Aop is exported from the nucleus and degraded after phosphorylation by mitogenactivated protein kinase (MAPK) (34). This regulation is essential for specification of R7 photoreceptors in the developing eye through receptor tyrosine kinase (RTK) signaling (35). We could not detect phosphorylated MAPK in Tm4 and Tm6 somas that strongly expressed Aop, but P-MAPK was present in Tm1 and Tm2, in which Aop protein could sometimes be observed as a "ring" outside the nucleus at P30 (fig. S7K, arrows), suggestive of nuclear export. This suggests that Drgx and Pdm3 initially repress Aop protein indirectly in Tm1 and Tm2, respectively, by rendering them sensitive to RTK signaling.

After P40, *aop* mRNA is also down-regulated in Tm1 and Tm2; this coincides with *Mef2* up-regulation in these cell types (fig. S7J) downstream of Pdm3 and Drgx (Figs. 1F and 2C). Knocking down *Mef2* using *TmX/Tm2-Gal4* resulted in a very rare (one out of 38 neu-

rons observed) conversion of Tm2 into Tm4 in adults, and 18% of Tm neurons observed were morphologically unrecognizable (Fig. 4, A and D). App could be detected in some of these cells, but only outside the nucleus (Fig. 4E), similar to wild-type Tm1 and Tm2 at P30 (fig. S7K). This indicates that aop was transcriptionally derepressed without Mef2, but its posttranslational repression through MAPK remained intact, even in adult brains. Therefore, aop appears to be down-regulated in Tm1 and Tm2 through two independent mechanisms (Fig. 4H): degradation of the protein through MAPK at all stages and transcriptional suppression by Mef2 after P40. Drgx and Pdm3 could control the first mechanism by regulating the expression of RTK genes such as InR, Ror, and Alk, which are differentially expressed between Tm1/2 and Tm4/6 clusters (fig. S7L).

Because pdm3 and Drgx both negatively regulate Aop expression (Figs. 1G and 2C), we investigated whether the opposite was also true. Overexpression of wild-type aop with TmX/Tm2-Gal4 did not convert Tm2 to either Tm4 or Tm6, but 25% of Tm neurons were morphologically unrecognizable (Fig. 4, A and D), similar to those observed with Mef2 RNAi, in which aop transcription was derepressed. These neurons still maintained Pdm3 (Fig. 4F), the coexpression of which with Aop might create a confused state. The signal for the ectopic Aop protein was weak (Fig. 4F), suggesting that it was being degraded by the active MAPK pathway in Tm2. We therefore overexpressed a constitutively active form of Aop (aop.ACT) that cannot be phosphorylated and degraded (34). In these brains, 40% of Tm2s were converted to Tm4s (Fig. 4, C and D) that had lost Pdm3 expression (Fig. 4G). This indicates that whereas Aop can suppress pdm3 and promote Tm4 fate (Fig. 4H, dashed arrow), this regulation is not relevant with wild-type aop because of RTK signaling, which ensures that *pdm3* acts upstream.

The apparent destabilization of the fate choice between Tm2 and Tm4 with the post-mitotic expression of *aopACT* (but not *aop.WT*) implies that neuronal identity remains dependent on the signaling conditions even after the initial specification events. Similar mechanisms in organisms with larger and more complex brains could be exploited to further diversify the neurons that are generated from the same stem cell pool with a common identity but then migrate to distinct brain regions where different signals might be available (*36*).

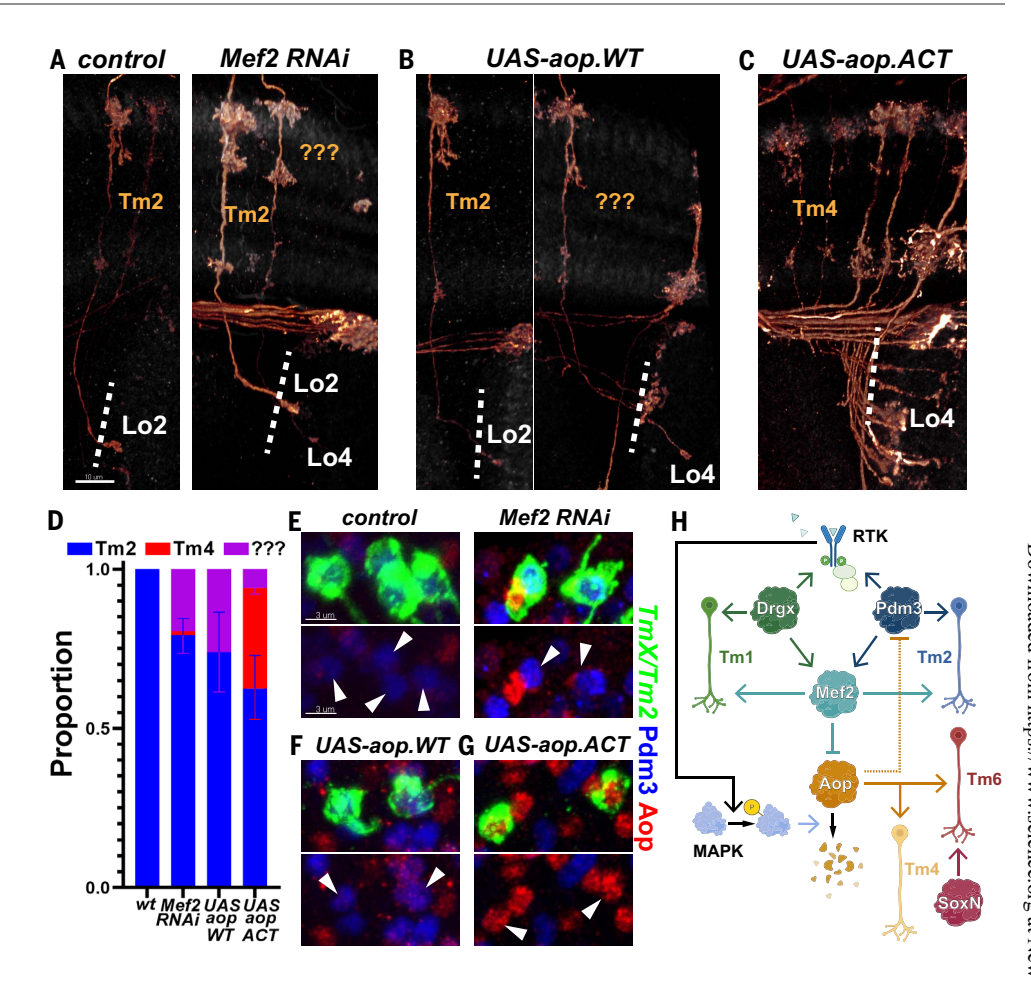
Decoding neuronal gene regulation through network inference

Cell-type identity encoded by terminal selectors represents only one aspect of neuronal gene regulation. Neuronal transcriptomes are dynamic throughout differentiation, typically in response to external signals such as the steroid hormone ecdysone (37–39). It remains unclear how these two top-level regulatory programs, i.e., the identity and developmental state, interact to combinatorially determine the expression of downstream genes in each neuron

We implemented the Inferelator 3.0 framework (40) to build gene regulatory network (GRN) models with the goal of gaining a more complete understanding of the regulatory programs used by developing optic lobe neurons. A key feature of this method is its use of transcription factor activity (TFA) that allows Inferelator to estimate the underlying activity of each TF using the expression levels of its known targets from prior information ("priors") (Fig. 5A). Calculating TFA before fitting a linear regression model to infer a GRN circumvents the issue that mRNA levels are often not a good substitute for a TF's latent activity (41), which may vary with posttranscriptional modifications or the presence of cofactors. We modeled GRNs in Tm1, Tm2, Tm4, and Tm6, as well as in the five types of lamina monopolar neurons (L1 to L5), which provide a useful benchmark for our models. For inference, we used single-cell transcriptomes from both our atlas (1) and one generated by another group (42) between the stages P24 and P50, when optic lobe neurons acquire most of their morphological features and begin to form synapses. We constructed priors for each network using the corresponding P48 clusters (fig. S6C) in the snATAC-seq dataset described above (28). Figure 5C displays the entire GRN inferred from the Tm neurons, highlighting the top 10 TFs with the highest number of targets predicted, which includes *Mef*2; the selectors *pdm3*, *cut*, and *ap*; as well as the ecdysone-responsive TFs Hr3, Hr39, Eip74EF, and Eip93F.

The scarcity of ground-truth networks presents a challenge when benchmarking inferred GRNs in complex multicellular organisms. To assess the predictive power of our models, we exploited available RNA-seq datasets collected from perturbed neurons. For lamina neurons, we used two relevant datasets: knockdown of Hr3 in all five lamina neurons at P48 (39) and L3 neurons at P40 mutant for erm (21). For Tm neurons, we used the UAS-pdm3 scRNAseq experiment that we performed at P50 (Fig. 1H). For each experiment, TFA was calculated using the same corresponding priors used for inference. We then applied matrix multiplication (dot product) between the estimated TFA and the learned weights between TFs and targets (betas) to generate a predicted expression matrix (fig. S8C). Even though these betas were determined from the completely independent, wild-type datasets discussed above, the real and predicted transcriptomes aligned

Fig. 4. RTK signaling stabilizes the Tm selector network. (A to G) TmX/Tm2-Gal4 driving CD4-tdGFP (flip-out) and Mef2 RNAi [(A) and (E)], UAS-aop.WT [(B) and (F)], or UAS-aop.ACT [(C) and (G)]. (A) to (C) 3D reconstructions of GFP for the representative adult neurons in each condition, with anti-NCad shown. "???" marks neurons that typically target to Lo4 but could not be recognized as any known optic lobe neuron on the basis of their morphology. Dashed lines mark the border of lobula neuropil. (D) Quantification of (A) to (C). n = 54/6 control, n = 38/8Mef2 RNAi, n = 16/6 aop.WT, and n =75/5 aop.ACT neurons/brains. P = 0.03(Mef2 RNAi), P = 0.02 (aop.WT), and P =0.005 (aop.ACT) for change in cell-type proportions. Error bars indicate SEM. (E) to (G) Same as (A) to (C), with maximum projections of somas with anti-Pdm3 shown in blue and anti-Aop shown in red. Arrowheads indicate GFP+ neurons. Scale bars: (A) to (C), 10 µm; (E) to (G), 3 µm. (**H**) Summary of the experimentally validated regulatory interactions between Drgx, Pdm3, Mef2, and Aop in Tm neurons. Negative regulation of Pdm3 by Aop (dashed line) is only applicable when Aop cannot be degraded through the MAPK pathway.



nearly perfectly according to their cell type and condition of origin (Fig. 5, D to F) after Seurat integration (43). However, we also observed that before integration (fig. S8E-G), the differences between control and perturbed conditions were much smaller in predicted clusters. Consistently, we found that the predicted transcriptomes recapitulated only a small proportion (10 to 30%) of the real DEGs between the control and perturbed conditions (low recall), but the predicted DEGs were mostly (>50%) correct (high precision) (fig. S8, H to J). Thus, our benchmarks suggest that the interactions learned by our models are largely accurate, although they represent only a snippet of the true underlying GRNs.

Selectors and ecdysone signaling regulate downstream targets

We found that nearly all of the regulatory relationships that we experimentally validated in the previous sections (Fig. 4H) were also captured by our GRN model (Fig. 5G), such as the regulation of *Mef2* by *Drgx* and *pdm3*. Drgx and Pdm3, although required, are not sufficient to activate *Mef2* expression, which does not occur until P40 despite the continuous expression of the selectors. Ecdysoneresponsive *Hr3* emerged as a candidate for

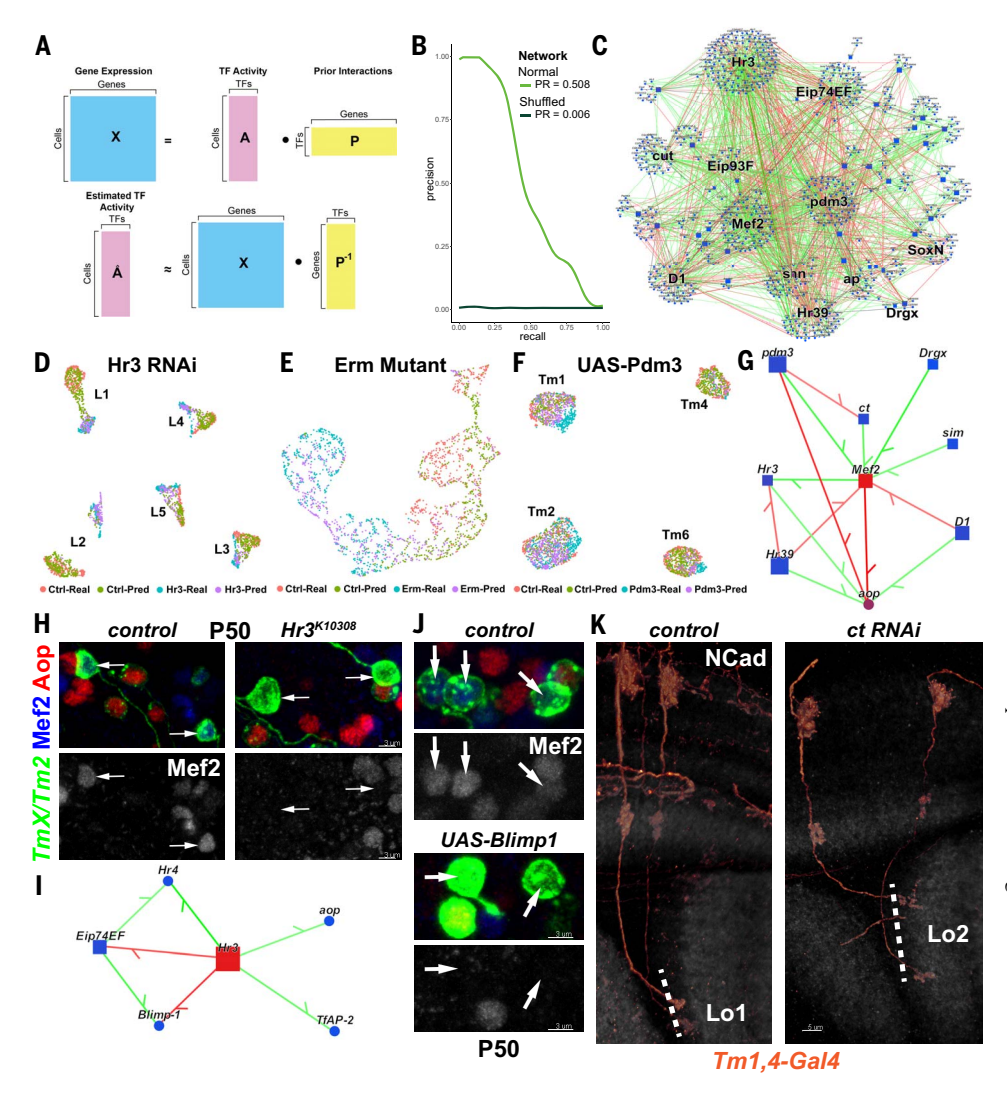
this temporal trigger because its activation around P30 precedes Mef2 (fig. S7J). We tested this prediction by generating Hr3 mutant MARCM clones using TmX/Tm2-Gal4. In adult brains, Mef2 expression was not affected, and Tm2 appeared morphologically normal (fig. S9A). However, at P50, Mef2 could not be detected in mutant clones (Fig. 5H), indicating that Mef2 expression was delayed but not abolished in Hr3 mutants. This implies that there are redundant temporal mechanisms regulating Mef2 expression and/or that Hr3acts indirectly to control Mef2. Among the predicted downstream targets of Hr3 (Fig. 5I), Hr4, Eip74EF, and Blimp-1 were all shown to be regulated by Hr3 in lamina neurons. the knockdown of which delays the downregulation of Blimp-1 (39), which normally occurs around P40 (fig. S7J). Indeed, overexpression of Blimp-1 using TmX/Tm2-Gal4 also repressed Mef2 at P50 (Fig. 5J), suggesting that Hr3 acts through Blimp-1 for this function. Our results show that the combinatorial action of the selectors Drgx/Pdm3 and the ecdysone-responsive TFs Hr3/Blimp-1 enables Mef2 to be expressed specifically in Tm1 and Tm2 and only after P40.

Another inferred edge in this subnetwork (Fig. 5G), the negative regulation of *cut* (*ct*) by

pdm3, was consistent with the lower levels of ct expression in Tm2 cluster compared with other Tm neurons (fig. S9B). Because different Cut expression levels in larval "da" sensory neurons regulate the size of their dendritic arborizations (44), this difference could be functionally significant. Indeed, we found that 73% of Tm1s targeted to the Lo2 layer instead of Lo1 upon ct knockdown (Fig. 5K). Thus, the level of ct expression controls a specific subroutine during brain wiring downstream of pdm3. However, overexpression of ct in Tm2 did not lead to their axons projecting to Lo1 instead of Lo2 (fig. S9C), suggesting that there are redundant mechanisms allowing Tm2 to arborize in this laver.

Finally, we inspected the GRN model of the Tm neurons (Fig. 5C) to assess whether different types of TFs specialize on different types of targets. We previously reported that TFs and cell surface proteins (CSPs) are overrepresented in DEGs between optic lobe neurons. CSPs are particularly up-regulated at P40 to P50 (1) during synaptogenesis. Accordingly, CSPs that may be involved in cell-cell recognition (45) were strongly enriched among the network targets (fig. S9D). However, we did not see a clear bias for any TF class to regulate more or fewer CSPs than others. We also performed Gene

Fig. 5. Computational inference of gene regulatory networks. (A) Gene expression in each cell is assumed to be a linear product of latent TF activities and the connectivity matrix (prior) between TFs and their targets (top). TFA is estimated as the dot product of the expression matrix and the pseudoinverse of the prior matrix (bottom). (B) Area under the precision-recall (AUPR) curves for the Tm network built using the MergedDA prior (see also fig. S6A). (C) Visualization of the network in (B), displaying all interactions with a minimum of 80% confidence (combined) and variance explained of 1%. Top 10 TFs that had the highest number of target genes in the network are highlighted in addition to SoxN and Drgx. (D to F) Single-cell transcriptomes of L1 to L5 at P48 expressing Hr3 RNAi (39) (D); simulated single L3 neurons (fig. S8D) at P40 mutant for erm (21) (E); and Tm1, Tm2, Tm4, and Tm6 at P50 overexpressing pdm3 (Fig. 1) (F). UMAPs were calculated using 30 PCs [(D) and (F)] or three PCs (E) on the integrated gene expression. (see also fig. S8, E to G). (G) Network visualization displaying all TFs predicted to regulate Mef2 or aop with confidence > 95%, and all inferred interactions between the displayed genes in the Tm network. Green indicates a positive correlation and red a negative correlation between mRNA levels of the gene pairs. (H) FRT42D and Hr3K10308 MARCM clones labeled with TmX/ Tm2-Gal4 and CD4-tdGFP in P50 medulla cortex (maximum projection), with anti-Mef2 shown in blue and anti-Aop shown in red. Arrows indicate Aop Tm neurons that should normally be $Mef2^+$ (n = 6 brains). (1) Same as (G), displaying all TFs predicted to be regulated



by Hr3 (confidence > 95%). (J) TmX/Tm2-Gal4 driving CD4-tdGFP (flip-out) and UAS-Blimp1 (n = 5 brains). Maximum projection is the same as in (H). (K) Tm1,4-Gal4 driving CD4-tdGFP (flip-out) and ct RNAi (n = 40/6 neurons/brains). 3D reconstructions of GFP for the representative adult neurons in each condition, with anti-NCad shown in white. Dashed lines mark the border of lobula neuropil. Scale bars: (H) to (J), 3 μ m; (K), 5 μ m.

Ontology (GO) term enrichment analysis on the predicted targets of the top three regulators in the network: ecdysone TF Hr3, the terminal selector Pdm3, and the effector TF Mef2. The same general terms were enriched for all of them: ion channels, cell adhesion, and signaling molecules (fig. S9E). These results further highlight the combinatorial nature of neuronal gene regulation, and they are consistent with other findings that most targets of the ecdysone-responsive TFs are cell-type specific (39) despite the uniform expression of these TFs in all neurons.

Discussion

We set out to test whether neuronal type identity is primarily encoded by unique and sustained combinations of TFs in each cell type. The terminal selector hypothesis has been extensively supported in *C. elegans*, and a few selectors have also been described in mice,

such as Fezf2 (homolog of Erm), the expression of which in cortical progenitors induces corticospinal motor neuron-like fates (15). However, the previous studies focused on the roles of individual selector genes and did not systematically test the sufficiency of a continuously expressed TF code in instructing all type-specific gene expression in neurons. We explicitly addressed this prediction by determining the selector codes of every neuron in the fly visual system using a developmental scRNA-seg atlas and by engineering predictable transformations between different neurons using only these TFs. This has so far been difficult to demonstrate, even in C. elegans, likely because neurons typically diverge by multiple selectors (46). Our results suggest that effector genes are controlled by different permutations of available selectors in each neuron, which implies that every effector might not be regulated by all selectors. Similar selector combinations generally resulted in similar transcriptomes and vice versa (fig. S1D), but this relationship was not strict, reflecting the combinatorial nature of TF action. For instance, during brain wiring (P50), we observed a distinct branch (fig. S2C, red circle) in which all annotated clusters corresponded to neurons that connect to the central brain irrespective of their developmental origin and the similarity of selector expression.

We defined terminal selectors broadly to satisfy two key criteria: continuous expression in postmitotic neurons and involvement in the control of neuronal type identity. It has also been proposed that selectors directly regulate most effector genes by binding to their cis-regulatory enhancers (47). In our GRN models (table S3), the interactions that were present in our prior network ("gold_standard=1")

represent those that were directly supported by cis-regulatory evidence, i.e., enrichment of motifs in differentially accessible regions near the target gene, and thereby indicate direct regulation. For instance, 27 of the 120 highconfidence targets of Pdm3 (fig. S9, D and E) have been supported by snATAC-seq to be direct interactions. This does not imply that all other interactions are indirect, because the Inferelator-Prior pipeline was designed to favor accuracy by only retaining the highest confidence targets for TFA calculation (40). These direct targets include several wiring molecules such as Dscam4 and the Netrin receptor frazzled, as well as effector TFs NK7.1 and CG9932. Consistently, overexpression of fra in Tm4s led to 54% of these neurons forming dendritic branches that split into a "fork" in the M2 layer, which is normally characteristic of Pdm3-expressing Tm2 (fig. S9F, arrowhead, compare with fig. S9C). Nevertheless, extensive utilization of effector TFs (such as Mef2 in Tm1 and Tm2) makes it likely that many targets are also regulated indirectly. Such transcriptional subroutines may be more prevalent in flies and higher organisms, in which neuronal differentiation occurs over several days or weeks, in contrast to worm neurons, which are typically functional within a few hours after their terminal division. Another feature that has been commonly, but not universally, associated with terminal selectors is autoregulation (47). Our results support that Pdm3 indeed autoactivates (Fig. 1, N and O), but this is unlikely to be the case for Drgx, SoxN, and Vsx1/2 given the lower efficiency of their overexpression (Fig. 2B and 3E and fig. S7A).

The apparent conservation of this regulatory logic in both C. elegans and Drosophila, the last common ancestor of which lived >600 million years ago (48), makes it likely that the terminal selector concept will also be useful for understanding and manipulating the neuronal diversity of mammalian brains. This could have large implications for the emerging field of cell replacement therapy. The usage of lineagespecific TFs for the generation of specific neuronal types in vitro have significantly improved the efficiency of these protocols (49). Some of these TFs, such as Pet1 and Lmx1b for serotonergic neurons (50) or Lmx1a and Nurr1 for dopaminergic neurons (51), are also likely to be terminal selectors. However, the protocols used still tend to produce heterogeneous populations of related cell types (52). We propose that more specific combinations of such reprogramming TFs could be identified in specific cell types of interest by virtue of their sustained postmitotic expression.

We found that the tTF *Klu* from neuroblasts activates the selector *Drgx* in newborn Tm1s, but we still know little about how the combined action of temporal, spatial, and Notch patterning (5) activates a unique set of selectors

in every neuronal type, and subsequently how the selector combination enacts precise gene batteries over the course of development. There are also some limitations of this framework. We and others previously reported that a few neuronal types have distinct transcriptomes during development but then converge to a common state in adult brains (1, 53). These are generally very similar (sub)types that only differ in their connectivity, so the TFs that encode their differences do not need to be maintained after their wiring is complete. In addition, TFs can be posttranscriptionally regulated by, e.g., the RNA-binding proteins Imp and Syp, which are widely used in Drosophila nervous system to generate neuronal diversity (54). This could complicate the identification of correct selector combinations from RNA-seq data alone.

Both this work and other previous efforts to decipher gene regulation in the fly brain (28) have now made it possible to study the molecular mechanisms of synaptic specificity within the framework of gene-regulatory mechanisms that encode neuronal type identity. We propose a "top-down" approach in which terminal selectors that cause broad changes in neuronal fates are identified first, followed by the dissection of downstream mechanisms aided by GRN modeling. Perhaps the most promising targets are effector TFs (e.g., cut) that still regulate many other genes but have more limited functions (subroutines) than the selectors. Nevertheless, the current models still have limitations, imposed mainly by the quality of snATAC-seq priors. Single-nucleus multiome studies that simultaneously profile gene expression and chromatin accessibility could remove many of these limitations in the near future.

Methods summary

Candidate terminal selectors

We selected for each neuronal cluster in our developmental scRNA-seq atlas (1) the TFs that were found as a consistent marker of that cluster or were continuously expressed at all stages according to binarized expression. We discarded all TFs that were expressed in >150 clusters (likely pan-neuronal).

The precise genotypes and temperatures used for experiments in each figure panel are detailed in table S4. Source details for all fly strains are specified in table S5. Full names of all genes referred to in the manuscript are listed in table S6.

Immunohistochemistry and RNA-FISH

Immunohistochemistry and RNA-fluorescence in situ hybridization (RNA-FISH) experiments were performed according to previously described protocols. New polyclonal antibodies were generated against Drgx, Pdm3, SoxN, Mef2, Vsx2, Brp, and Repo by Genscript. Source details for all other antibodies are specified in table S5. Custom FISH probes were designed by Molecular Instruments against the transcripts of 5-HT7, $Oct\beta IR$, Or63a, and Dh44-R1. All samples were imaged using a Leica SP8 confocal microscope with a 63× (numerical aperture 1.3) glycerol objective. Images were analyzed using Imaris (for details, see the supplementary materials). Parametric, two-sided t tests were used for all pairwise comparisons. Drgx^{ΔTm1} deletion was produced by WellGenetics through CRISPR-mediated mutagenesis.

scRNA-seq

We labeled all four Tm neurons (TmX/Tm2-Gal4) with nuclear green fluorescent protein, crossed to either UAS-pdm3 or yw (control), isolated the labeled cells using fluorescenceactivated cell sorting (FACS), prepared libraries using the 10x Genomics 3' kit (v3.1), and then sequenced them on the Illumina NovaSeq 6000 platform. The data were analyzed with CellRanger v5 and Seurat v4.

Network inference

We used a published snATAC-seq dataset (28) to identify differentially accessible regions between the Tm1, Tm2, Tm4, and Tm6 clusters (the Tm network) and L1 to L5 clusters (the lamina network) at P48. We then used the Inferelator-Prior v0.2.3 faf5e47 package to scan and score these regions within 10 kb of every gene for TF-binding motifs. The scores were then clustered to retain only the highest confidence targets of each TF for TFA calculation. For inference, we used single-cell transcriptomes from (1) at stages P30, P40, and P50 and from (42) at stages P24, P36, and P48. The networks were modeled only on the genes that displayed differential expression between either the cell types or the time points analyzed using Inferelator 3 (v0.5.6 dd532f4). The network performances were evaluated against the respective priors using four different metrics (fig. S8 and materials and methods). We additionally compared the performance of each network with negative control networks that were built with shuffled priors.

REFERENCES AND NOTES

- 1. M. N. Özel et al., Neuronal diversity and convergence in a visual system developmental atlas, Nature 589, 88-95 (2021). doi: 10.1038/s41586-020-2879-3; pmid: 33149298
- K. F. Fischbach, A. P. M. Dittrich, The optic lobe of Drosophila melanogaster. I. A Golgi analysis of wild-type structure. Cell Tissue Res. 258, 441-475 (1989). doi: 10.1007/
- 3. K. T. Ngo, I. Andrade, V. Hartenstein, Spatio-temporal pattern of neuronal differentiation in the Drosophila visual system: A user's guide to the dynamic morphology of the developing optic lobe. Dev. Biol. 428, 1-24 (2017). doi: 10.1016/ i.vdbio.2017.05.008; pmid: 28533086
- F. Yu, C. T. Kuo, Y. N. Jan, Drosophila neuroblast asymmetric cell division: Recent advances and implications for stem cell biology. Neuron 51, 13-20 (2006). doi: 10.1016/ j.neuron.2006.06.016; pmid: 16815328

- T. Erclik et al., Integration of temporal and spatial patterning generates neural diversity. Nature 541, 365–370 (2017). doi: 10.1038/nature20794; pmid: 28077877
- N. Konstantinides et al., A complete temporal transcription factor series in the fly visual system. Nature 604, 316–322 (2022). doi: 10.1038/s41586-022-04564-w; pmid: 35388222
- X. Li et al., Temporal patterning of Drosophila medulla neuroblasts controls neural fates. Nature 498, 456–462 (2013). doi: 10.1038/nature12319; pmid: 23783517
- I. Holguera, C. Desplan, Neuronal specification in space and time. Science 362, 176–180 (2018). doi: 10.1126/science. aas9435; pmid: 30309944
- O. Hobert, "Terminal selectors of neuronal identity," in Current Topics in Developmental Biology, P. M. Wassarman, Ed. (Academic, 2016), vol. 116, pp. 455–475.
- E. G. Berghoff et al., The Prop1-like homeobox gene unc-42 specifies the identity of synaptically connected neurons. eLife 10, e64903 (2021). doi: 10.7554/eLife.64903; pmid: 34165428
- L. Pereira et al., A cellular and regulatory map of the cholinergic nervous system of C. elegans. eLife 4, e12432 (2015), doi: 10.7554/elife.12432; pmid: 26705699
- N. Stefanakis, I. Carrera, O. Hobert, Regulatory Logic of Pan-Neuronal Gene Expression in C. elegans. Neuron 87, 733–750 (2015). doi: 10.1016/j.neuron.2015.07.031; pmid: 26291158
- E. Serrano-Saiz, E. Leyva-Díaz, E. De La Cruz, O. Hobert, BRN3-type POU homeobox genes maintain the identity of mature postmitotic neurons in nematodes and mice. *Curr. Biol.* 28, 2813–2823.e2 (2018). doi: 10.1016/j.cub.2018.06.045; pmid: 30146154
- L. Remesal et al., PBX1 acts as terminal selector for olfactory bulb dopaminergic neurons. Development 147, dev.186841 (2020). doi: 10.1242/dev.186841; pmid: 32156753
- S. Lodato et al., Gene co-regulation by Fezf2 selects neurotransmitter identity and connectivity of corticospinal neurons. Nat. Neurosci. 17, 1046–1054 (2014). doi: 10.1038/ nn.3757; pmid: 24997765
- P. Arlotta, O. Hobert, Homeotic transformations of neuronal cell identities. *Trends Neurosci.* 38, 751–762 (2015). doi: 10.1016/j.tins.2015.10.005; pmid: 26596501
- M. B. Reilly, C. Cros, E. Varol, E. Yemini, O. Hobert, Unique homeobox codes delineate all the neuron classes of C. elegans. *Nature* 584, 595–601 (2020). doi: 10.1038/s41586-020-2618-9; pmid: 32814896
- E. Hasegawa, M. Kaido, R. Takayama, M. Sato, Brain-specific-homeobox is required for the specification of neuronal types in the *Drosophila* optic lobe. *Dev. Biol.* 377, 90–99 (2013). doi: 10.1016/j.ydbio.2013.02.012; pmid: 23454478
- E. Hasegawa et al., Concentric zones, cell migration and neuronal circuits in the *Drosophila* visual center. *Development* 138, 983–993 (2011). doi: 10.1242/dev.058370; pmid: 21303851
- T. Suzuki et al., Formation of neuronal circuits by interactions between neuronal populations derived from different origins in the *Drosophila* visual center. *Cell Rep.* 15, 499–509 (2016). doi: 10.1016/j.celrep.2016.03.056; pmid: 27068458
- J. Peng et al., Drosophila Fezf coordinates laminar-specific connectivity through cell-intrinsic and cell-extrinsic mechanisms. eLife 7, e33962 (2018). doi: 10.7554/eLife.33962; pmid: 29513217
- T. Schilling, A. H. Ali, A. Leonhardt, A. Borst, J. Pujol-Martí, Transcriptional control of morphological properties of directionselective T4/T5 neurons in *Drosophila*. *Development* 146, dev169763 (2019). doi: 10.1242/dev.169763; pmid: 30642835
- T. Lee, L. Luo, Mosaic analysis with a repressible cell marker (MARCM) for *Drosophila* neural development. *Trends Neurosci.* 24, 251–254 (2001). doi: 10.1016/S0166-2236(00)01791-4; pmid: 11311363
- C.-K. Chen, W.-Y. Chen, C.-T. Chien, The POU-domain protein Pdm3 regulates axonal targeting of R neurons in the *Drosophila* ellipsoid body. *Dev. Neurobiol.* 72, 1422–1432 (2012). doi: 10.1002/ dneu.22003; pmid: 22190420
- A. L. Tichy, A. Ray, J. R. Carlson, A new *Drosophila* POU gene, pdm3, acts in odor receptor expression and axon targeting of olfactory neurons. J. Neurosci. 28, 7121–7129 (2008). doi: 10.1523/JNEUROSCI.2063-08.2008; pmid: 18614681
- Y. Togane et al., Spatio-temporal pattern of programmed cell death in the developing *Drosophila* optic lobe. *Dev. Growth Differ.* 54, 503–518 (2012). doi: 10.1111/j.1440-169X.2012.01340.x; pmid: 22587328

- Z. Song, K. McCall, H. Steller, DCP-1, a Drosophila cell death protease essential for development. Science 275, 536–540 (1997). doi: 10.1126/science.275.5299.536; pmid: 8999799
- J. Janssens et al., Decoding gene regulation in the fly brain. Nature 601, 630–636 (2022). doi: 10.1038/s41586-021-04262-z; pmid: 34987221
- T. Suzuki, M. Kaido, R. Takayama, M. Sato, A temporal mechanism that produces neuronal diversity in the *Drosophila* visual center. *Dev. Biol.* 380, 12–24 (2013). doi: 10.1016/ j.ydbio.2013.05.002; pmid: 23665475
- J. Morante, C. Desplan, The color-vision circuit in the medulla of *Drosophila*. *Curr. Biol.* 18, 553–565 (2008). doi: 10.1016/ j.cub.2008.02.075; pmid: 18403201
- A. T. Chao, W. M. Jones, A. Bejsovec, The HMG-box transcription factor SoxNeuro acts with Tcf to control Wg/Wnt signaling activity. Development 134, 989–997 (2007). doi: 10.1242/ dev.02796; pmid: 17267442
- M. Schober, I. Rebay, N. Perrimon, Function of the ETS transcription factor Yan in border cell migration. *Development* 132, 3493–3504 (2005). doi: 10.1242/dev.01911; pmid: 16014514
- F. P. Davis et al., A genetic, genomic, and computational resource for exploring neural circuit function. eLife 9, e50901 (2020). doi: 10.7554/eLife.50901; pmid: 31939737
- I. Rebay, G. M. Rubin, Yan functions as a general inhibitor of differentiation and is negatively regulated by activation of the Ras1/MAPK pathway. Cell 81, 857–866 (1995). doi: 10.1016/ 0092-8674(95)90006-3; pmid: 7781063
- E. M. O'Neill, I. Rebay, R. Tjian, G. M. Rubin, The activities of two Ets-related transcription factors required for *Drosophila* eye development are modulated by the Ras/MAPK pathway. *Cell* 78, 137–147 (1994). doi: 10.1016/0092-8674(94)90580-0; pmid: 8033205
- C. Mayer et al., Developmental diversification of cortical inhibitory interneurons. *Nature* 555, 457–462 (2018). doi: 10.1038/nature25999; pmid: 29513653
- K. P. White, P. Hurban, T. Watanabe, D. S. Hogness, Coordination of *Drosophila* metamorphosis by two ecdysoneinduced nuclear receptors. *Science* 276, 114–117 (1997). doi: 10.1126/science.276.5309.114; pmld: 9082981
- L. M. Riddiford, J. W. Truman, A. Nern, Juvenile hormone reveals mosaic developmental programs in the metamorphosing optic lobe of *Drosophila melanogaster*. *Biol. Open* 7, bio034025 (2018). doi: 10.1242/bio.034025; pmid: 29618455
- S. Jain et al., A global timing mechanism regulates cell-typespecific wiring programmes. *Nature* 603, 112–118 (2022). doi: 10.1038/s41586-022-04418-5; pmid: 35197627
- C. Skok Gibbs et al., High-performance single-cell gene regulatory network inference at scale: The Inferelator 3.0. Bioinformatics 38, 2519–2528 (2022). doi: 10.1093/bioinformatics/btac117; pmid: 35188184
- T. Schacht, M. Oswald, R. Eils, S. B. Eichmüller, R. König, Estimating the activity of transcription factors by the effect on their target genes. *Bioinformatics* 30, i401–i407 (2014). doi: 10.1093/bioinformatics/btu446; pmid: 25161226
- Y. Z. Kurmangaliyev, J. Yoo, J. Valdes-Aleman, P. Sanfilippo,
 L. Zipursky, Transcriptional programs of circuit assembly in the *Drosophila* visual system. *Neuron* 108, 1045–1057.e6 (2020). doi: 10.1016/j.neuron.2020.10.006; pmid: 33125872
- T. Stuart *et al.*, Comprehensive integration of single-cell data. *Cell* 177, 1888–1902.e21 (2019). doi: 10.1016/j.cell.2019.05.031; pmid: 31178118
- W. B. Grueber, L. Y. Jan, Y. N. Jan, Different levels of the homeodomain protein cut regulate distinct dendrite branching patterns of *Drosophila* multidendritic neurons. *Cell* 112, 805–818 (2003). doi: 10.1016/S0092-8674(03)00160-0; pmid: 12654247
- M. Kurusu et al., A screen of cell-surface molecules identifies leucine-rich repeat proteins as key mediators of synaptic target selection. Neuron 59, 972–985 (2008). doi: 10.1016/ j.neuron.2008.07.037; pmid: 18817735
- P. Kratsios et al., An intersectional gene regulatory strategy defines subclass diversity of C. elegans motor neurons. eLife 6, e25751 (2017). doi: 10.7554/eLife.25751; pmid: 28677525
- O. Hobert, P. Kratsios, Neuronal identity control by terminal selectors in worms, flies, and chordates. *Curr. Opin. Neurobiol.* 56, 97–105 (2019). doi: 10.1016/j.conb.2018.12.006; pmid: 30665084

- T. A. Holton, D. Pisani, Deep genomic-scale analyses of the metazoa reject Coelomata: Evidence from single- and multigene families analyzed under a supertree and supermatrix paradigm. *Genome Biol. Evol.* 2, 310–324 (2010). doi: 10.1093/ gbe/evq016; pmid: 20624736
- M. Fitzgerald, N. Sotuyo, D. J. Tischfield, S. A. Anderson, Generation of cerebral cortical GABAergic interneurons from pluripotent stem cells. Stem Cells 38, 1375–1386 (2020). doi: 10.1002/stem.3252; pmid: 32638460
- Z. Xu et al., Direct conversion of human fibroblasts to induced serotonergic neurons. Mol. Psychiatry 21, 62–70 (2016). doi: 10.1038/mp.2015.101; pmid: 26216300
- M. Caiazzo et al., Direct generation of functional dopaminergic neurons from mouse and human fibroblasts. Nature 476, 224–227 (2011). doi: 10.1038/nature10284; pmid: 21725324
- N. Konstantinides, C. Desplan, Neuronal differentiation strategies: Insights from single-cell sequencing and machine learning. *Development* 147, dev193631 (2020). doi: 10.1242/ dev.193631; pmid: 33293292
- H. Li et al., Classifying Drosophila olfactory projection neuron subtypes by single-cell RNA sequencing. Cell 171, 1206–1220.e22 (2017). doi: 10.1016/j.cell.2017.10.019; pmid: 29149607
- A. M. Rossi, C. Desplan, Extrinsic activin signaling cooperates with an intrinsic temporal program to increase mushroom body neuronal diversity. *eLife* 9, e58880 (2020). doi: 10.7554/ eLife.58880; pmid: 32628110

ACKNOWLEDGMENTS

We thank all members of the Desplan and Bonneau laboratories: O. Hobert, R. Mann, and D. Jabaudon for helpful discussions; C. Doe, S. Aerts, J. Blau, E. Mazzoni, R. Hiesinger, N. Konstantinides D. Chen, R. Loker, and S. Mukherjee for critical reading of the manuscript; D. Krantz, I. Rebay, C.-T. Chien, W. Grueber, and J. Rister for reagents; Y.-C. Chen for help with plotting; J. Janssens and S. Aerts for sharing the snATAC-seq data ahead of publication; and G.-A. Saldi for help with network inference. Funding: This work was supported by the National Institutes of Health (NIH grants EY13010 and EY017916 to C.D. and R01HD096770, R01CA229235 and RM1HG011014 to R.B.) and the Simons Foundation. M.N.O. was a Leon Levy Neuroscience Fellow and is supported by the National Institute of Neurological Disorders and Stroke (NIH grant K99NS125117). C.S.G. is supported by National Science Foundation award 1922658 to the New York University Center for Data Science. I.H. has been supported by Human Frontier Science Program Postdoctoral Fellowship LT000757/2017-L and by a senior postdoctoral fellowship from the Kimmel Center for Stem Cell Biology. Author contributions: M.N.O., R.B., and C.D. conceived the project. M.N.O. designed all experiments. C.S.G. developed and optimized the Inferelator workflows. M.N.O., I.H., and M.S. performed the experiments. M.N.O. and C.S.G. analyzed the data. M.N.O., C.S.G., and C.D. wrote the manuscript. All authors edited the manuscript. Competing interests: The authors declare no competing interests Data availability: All data supporting the conclusions in this manuscript can be found in the main text or the supplemental materials. Raw and processed scRNA-seq data are publicly accessible on GEO with identifier GSE199734). Newly created materials from this study may be requested from the corresponding authors. License information: Copyright © 2022 the authors, some rights reserved; exclusive licensee American Association for the Advancement of Science. No claim to original US government works. https://www. science.org/about/science-licenses-journal-article-reuse

SUPPLEMENTARY MATERIALS

science.org/doi/10.1126/science.add1884 Materials and Methods Figs. S1 to S9 Tables S1 to S6 FACS Gating Strategy References (55–66) MDAR Reproducibility Checklist

View/request a protocol for this paper from Bio-protocol.

Submitted 25 May 2022; accepted 17 November 2022 Published online 8 December 2022 10.1126/science.add1884



Coordinated control of neuronal differentiation and wiring by sustained transcription factors

Mehmet Neset zel, Claudia Skok Gibbs, Isabel Holguera, Mennah Soliman, Richard Bonneau, and Claude Desplan

Science, **378** (6626), eadd1884. DOI: 10.1126/science.add1884

Generating neuronal diversity

Neurons in the brain seem to come in a dizzying array of diversity. Özel *et al.* found that the identities of nearly 200 different neurons in *Drosophila* fruit flies are set from a combinatorial code of only about 10 transcription factors. Modified expression of certain transcription factors drives predictable changes on neuronal cell fates, and these transcription factors intersect with hormone signaling to control brain wiring. —PJH

View the article online

https://www.science.org/doi/10.1126/science.add1884 **Permissions**

https://www.science.org/help/reprints-and-permissions

Use of this article is subject to the Terms of service